

Observation of two-neutrino double electron capture in ¹²⁴Xe with XENON1T

XENON Collaboration*

Two-neutrino double electron capture (2 ν ECEC) is a secondorder weak-interaction process with a predicted half-life that surpasses the age of the Universe by many orders of magnitude¹. Until now, indications of 2ν ECEC decays have only been seen for two isotopes²⁻⁵, ⁷⁸Kr and ¹³⁰Ba, and instruments with very low background levels are needed to detect them directly with high statistical significance^{6,7}. The 2ν ECEC half-life is an important observable for nuclear structure models⁸⁻¹⁴ and its measurement represents a meaningful step in the search for neutrinoless double electron capture—the detection of which would establish the Majorana nature of the neutrino and would give access to the absolute neutrino mass^{15–17}. Here we report the direct observation of 2ν ECEC in ¹²⁴Xe with the XENON1T dark-matter detector. The significance of the signal is 4.4 standard deviations and the corresponding half-life of 1.8×10^{22} years (statistical uncertainty, 0.5×10^{22} years; systematic uncertainty, 0.1×10^{22} years) is the longest measured directly so far. This study demonstrates that the low background and large target mass of xenon-based dark-matter detectors make them well suited for measuring rare processes and highlights the broad physics reach of larger next-generation experiments 18-20.

The long half-life of double electron capture makes it extremely rare, and the process has escaped detection for decades. In 2ν ECEC, two protons in a nucleus are simultaneously converted into neutrons by the absorption of two electrons from one of the atomic shells and the emission of two electron neutrinos 1 (ν_e). After the capture of the two atomic electrons, mostly from the K shell 21 , the filling of vacancies results in a detectable cascade of X-rays and Auger electrons 22 . The nuclear binding energy Q released in the process (on the order of 1 MeV) is carried away mostly by the two neutrinos, which are not detected within the detector. Thus, the experimental signature appears in the kiloelectronvolt, rather than the megaelectronvolt, range. The process is illustrated in Fig. 1.

 $2\nu ECEC$ is allowed in the standard model of particle physics and is related to double β decay as a second-order weak-interaction process. However, few experimental indications exist. Geochemical studies 4,5 for $^{130} Ba$ and a direct measurement 2,3 for $^{78} Kr$ quote half-lives of the order of $10^{20}-10^{22}$ yr.

Even longer timescales are expected for a hypothetical double electron capture without neutrino emission $(0\nu\text{ECEC})^{16,17}$. A detection of this decay would show that neutrinos are Majorana particles¹⁵ (that is, their own anti-particles) and could help us to understand the dominance of matter over antimatter in our Universe by means of leptogenesis²³. A Majorana nature would give access to the absolute neutrino mass, but only with theoretical nuclear-matrix-element calculations. A plethora of different nuclear models^{8–14} can also be applied to predict the $2\nu\text{ECEC}$ half-life; thus, its measurement would provide a vital experimental constraint for these models, as well as insight into double- β -decay processes on the proton-rich side of the nuclide chart.

Here we study the 2ν ECEC decay of 124 Xe. Natural xenon is a radiopure and scalable detector medium that contains about 1 kg of 124 Xe per tonne. 124 Xe undergoes 2ν ECEC to 124 Te with 24 Q = 2,857 keV. Because the amount of energy released by the recoiling nucleus is negligible (on the order of $10\,\mathrm{eV}$) and the neutrinos carrying away the energy Q are undetected, only the X-rays and Auger electrons are measured. The total energy for double K-shell-electron capture 24 is 64.3 keV. This value has already been corrected for energy depositions that do not exceed the xenon excitation threshold 22 . Previous searches for the $2\nu\text{ECEC}$ decay of ^{124}Xe were carried out with gas proportional counters using enriched xenon 6 , as well as large detectors originally designed for dark-matter searches 25 . The currently leading lower limit on the half-life of this decay comes from the XMASS collaboration at $T_{1/2}^{2\nu\text{ECEC}} > 2.1 \times 10^{22}$ yr (90% confidence level) 7 .

XENON1T²⁶ was built to detect interactions of dark matter in the form of weakly interacting massive particles (WIMPs) and has recently placed the most stringent limits on the coherent elastic scattering of WIMPs with xenon nuclei²⁷. XENON1T uses 3.2 t of ultra-pure liquid xenon (LXe), of which 2 t are within the sensitive volume of the time-projection chamber (TPC): a cylinder with diameter and height of about 96 cm and with walls of highly reflective polytetrafluoroethylene, equipped with 248 photomultiplier tubes (PMTs). The TPC is used for the measurement of the scintillation (S1) and ionization signals (S2) induced by particle interactions—the latter by converting ionization electrons into light by means of proportional scintillation. It provides calorimetry and three-dimensional position reconstruction and measures the scatter multiplicity.

The detector is shielded by the overburden due to its underground location at Laboratori Nazionali del Gran Sasso, by an active water Cherenkov muon veto 28 and by the LXe itself. All detector materials were selected to have low amounts of radioactive impurities and low radon emanation rates 29 . In addition, the anthropogenic β -emitter ^{85}Kr was removed from the xenon inventory by cryogenic distillation 30 . The combination of material selection, active background reduction and selection of an inner low-background fiducial volume in the data analysis results in an extremely low event rate of about 80 events $keV^{-1}\,t^{-1}\,yr^{-1}$. This makes XENON1T the most sensitive detector for $2\nu ECEC$ searches in ^{124}Xe at present.

The data presented here were recorded between 2 February 2017 and 8 February 2018 as part of a dark-matter search. Details on the detector conditions and signal corrections can be found in the original publication²⁷. The data quality criteria from the dark-matter analysis were applied, with the exception of those exhibiting low acceptance in the energy region of interest, around 60 keV. During the analysis, the data were blinded (that is, inaccessible for analysis) from 56 keV to 72 keV and unblinded only after the data quality criteria, fiducial volume and background model had been fixed. Datasets acquired after detector calibrations with an external ²⁴¹AmBe neutron source or a deuterium– deuterium-fusion neutron generator were removed to reduce the impact of radioactive ¹²⁵I, which was produced by the activation of ¹²⁴Xe during neutron calibrations and was taken out within a few days using the purification system. A pre-unblinding quantification of this removal using short-term calibration data led to a first reduction of the dataset to a live time of 214.3 d. This dataset was used to construct the background model. After unblinding, the long-term behaviour of ¹²⁵I

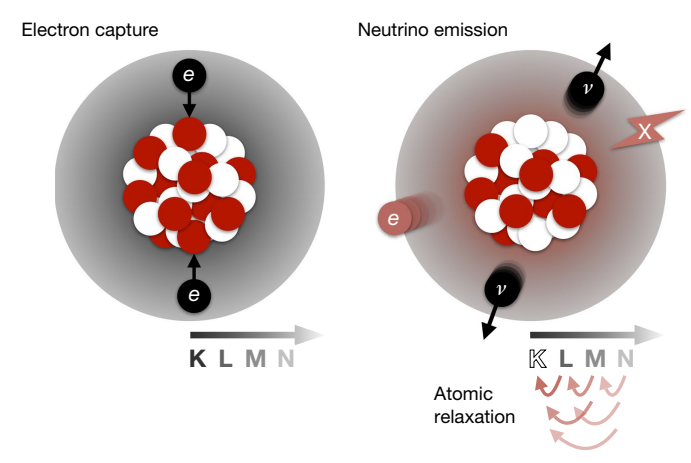


Fig. 1 | Schematic of two-neutrino double electron capture. In the 2ν ECEC process the nucleus captures two atomic-shell electrons (black), usually from the K shell, and simultaneously converts two protons (red) to neutrons (white). Two neutrinos (black) are emitted in the nuclear process and carry away most of the decay energy while the atomic shell is left in an excited state with two holes in the K shell. A cascade of X-rays (red, 'X') and Auger electrons (red, 'e') are emitted during atomic relaxation, when the K shell is refilled from the higher-energy L, M and N shells. In turn, vacancies are created in the refilling shells and are refilled with electrons from the higher-energy shells (arrows).

could be quantified and led to a further removal of datasets (Methods). This yielded a final live time of 177.7 d.

Atomic X-rays and Auger electrons cannot be resolved individually owing to their sub-millimetre range in LXe and the rapid succession of the relevant atomic processes. Therefore, the experimental signature of K-shell 2ν ECEC in XENON1T is a single S1 + S2 pair. Both S1 and S2 signals were used for the analysis to achieve the optimal energy resolution for the resulting peak. The energy scale around the expected signal at $E_0 = (64.3 \pm 0.6)$ keV was calibrated using monoenergetic lines of injected calibration sources (for example, 83mKr), neutron-activated xenon isotopes and γ -rays from radioactive decays in the detector materials. The energy resolution of a Gaussian peak at E_0 is $\sigma/\mu = (4.1 \pm 0.4)\%$, where μ is the energy and σ is the width of the peak (Methods). The uncertainty on E_0 reflects the uncertainties of both the energy reconstruction and the correction for sub-excitation quanta. An ellipsoidal 1.5-t inner fiducial mass was identified as providing the optimal signal-to-background ratio in sideband studies between 80 keV and 140 keV, above the blinded signal region.

Understanding the measured energy spectrum is essential when searching for a small peak from 2ν ECEC. Three classes of backgrounds contribute to the spectrum: from intrinsic radioactive isotopes that are mixed with the LXe, from radioactive isotopes in the detector materials and from solar neutrinos. The latter is subdominant and well constrained from solar and nuclear physics. γ -rays from 60 Co and 40 K, as well as from ²³⁸U and ²³²Th decay chains, constitute the bulk of the detector material backgrounds. They can undergo forward Compton scattering before entering the 2.0-t active mass and produce a flat spectrum at low energies. Multiple scatters inside the active volume are rejected by selecting events with only a single S2 compatible with a single S1. The most important intrinsic background components are β decays of ²¹⁴Pb, a daughter of ²²²Rn that is emanated from inner surfaces in contact with xenon, the two-neutrino double β decay of $^{136}\mbox{Xe}$ and the β decay of $^{85}\mbox{Kr}.$ Monoenergetic peaks from $^{83m}\mbox{Kr}$ injected for calibration and activation peaks that occur after neutron calibrations ($^{131\text{m}}$ Xe and $^{129\text{m}}$ Xe) are present in the spectrum as well. The activation 124 Xe + $n \rightarrow ^{125}$ Xe + γ has implications for 2ν ECEC search, as 125 Xe decays to 125 I via electron capture. With a branching ratio of 100% and a half-life of 59.4 d, ¹²⁵I decays into an excited state of ¹²⁵Te. The subsequently emitted γ -ray together with the K-shell X-ray, which is produced in 87.5% of cases, leads to a monoenergetic peak at 67.3 keV. Owing to its proximity to E_0 , this peak would present a large background

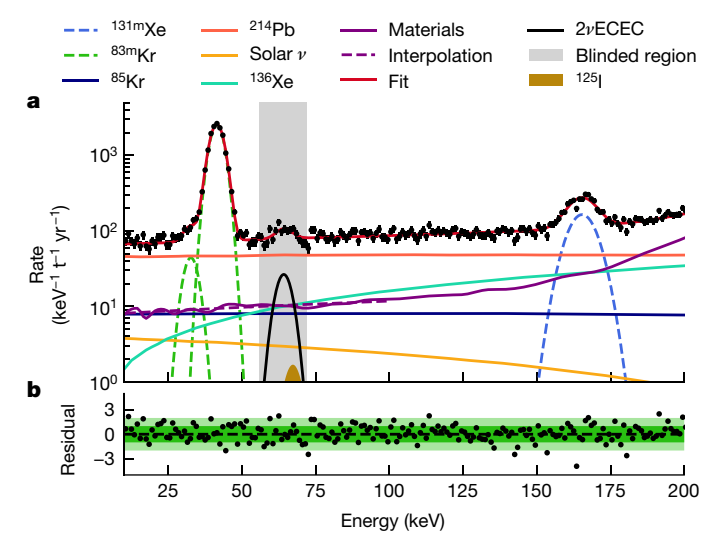


Fig. 2 | Fit of the background model to the measured energy spectrum. The exposure of the background data is 177.7 d in the 1.5-t inner fiducial mass and the uncertainties are Poissonian. a, The data are described by a simultaneous fit of Monte Carlo-generated background spectra, taking into account all known background sources and the $2\nu ECEC$ signal (solid red line; $\chi^2/\text{d.o.f.}\approx527.3/462$; d.o.f., degrees of freedom) in two subvolumes of the detector (Methods). The linear interpolation of the detector material backgrounds below 100 keV is indicated by the purple dashed line. The remaining intrinsic background sources are shown as solid and dashed coloured lines. The energy region around the expected $2\nu ECEC$ peak was blinded (grey band) until the background model was defined. b, The residuals between the data and the fit, including the 1σ (2σ) bands, are shown in green (light green).

for the 2 ν ECEC search that would only become apparent after unblinding. Using an activation model based on the parent isotope, we verified that $^{125}\mathrm{I}$ was removed from the detector with a time constant of $\tau=(9.1\pm2.6)$ d (Methods). This is in accordance with continuous xenon purification using hot zirconium getters 26 . Accounting for artificial neutron activation from calibrations and for activation by radiogenic thermal neutrons in the purification loop outside the water tank, we expect $N_{125_1}=(10\pm7)$ events in the 177.7-d dataset.

The background model was constructed by matching Monte Carlo simulations of all known background components 18 with the measured energy spectrum. Taking into account the finite detector resolution, events with single energy depositions in the active volume were selected from the Monte Carlo data and convolved with the measured energy resolution. The weighted sum of all spectra was optimized simultaneously to resemble the measured energy spectrum (Methods). The blinded signal region was not used in the fit. The measured energy spectrum with the best fits for the individual components is shown in Fig. 2. After unblinding of the signal region, a clear peak at E_0 was identified. The energy and signal width obtained from the spectral fit to the unblinded data are $\mu = (64.2 \pm 0.5)$ keV and $\sigma = (2.6 \pm 0.3)$ keV, respectively. The resulting sum spectrum of the event rate is shown in Fig. 3. Converting the fit to the total event count yields $N_{125} = (9 \pm 7)$ events from the decay of ¹²⁵I and $N_{2\nu \text{ECEC}} =$. (126 \pm 29) events from 2 ν ECEC. Compared to the null hypothesis, the $\sqrt{\Delta \chi^2}$ value of the best fit is 4.4.

Several consistency checks were carried out. We verified that the signal was homogeneously distributed in space and accumulated linearly with the exposure. A simultaneous fit of an inner (1.0 t) and an outer (0.5 t) detector mass with different background compositions yielded consistent signal rates. We verified the linearity of the energy calibration by identifying the 125 I activation peak at its expected position, which is separated from E_0 by more than the energy resolution.

The fit accounts for systematic uncertainties, such as cut acceptance and the number of ¹²⁵I events, by including them as fit-parameter

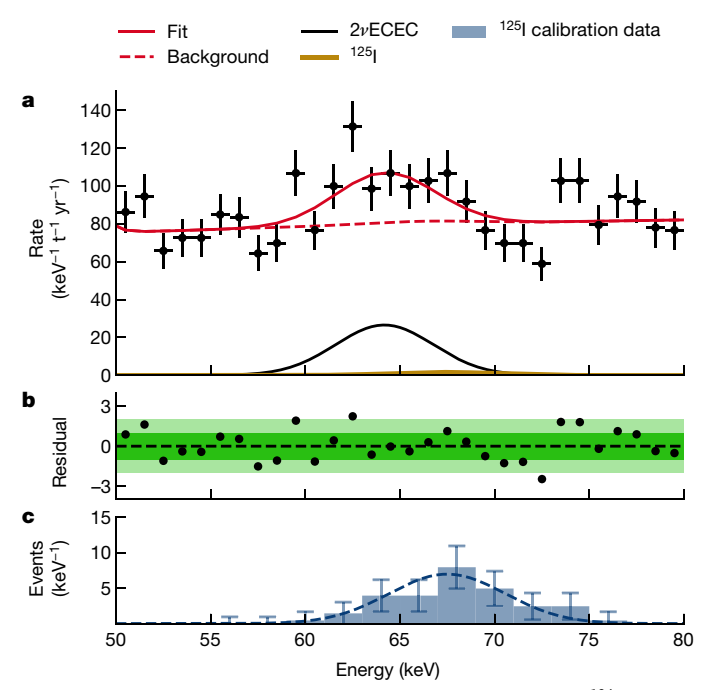


Fig. 3 | Zoom on the energy region of interest for 2ν ECEC in 124 Xe. a, The best-fit contribution from 2ν ECEC with $N_{2\nu$ ECEC} = 126 events is shown by the solid black line and the full fit is indicated by the solid red line. The peak from 125 I with $N_{125_1} = 9$ events is indicated by the solid gold line. The background-only model without 2ν ECEC (red dashed line), again over the full-fit range, clearly does not describe the data. The error bars indicate Poisson uncertainties. b, Residuals for the best fit are given with the 1σ (2σ) band indicated in green (light green). c, A histogram of the 125 I activation peak as seen in 6 d of data after a dedicated neutrongenerator calibration. The Poisson uncertainties (error bars) of the data were calculated before a linear background was subtracted. The peak shows the expected shift with respect to the 2ν ECEC signal. The blue dashed line indicates a binned likelihood fit of the Gaussian peak.

constraints. Additional systematic uncertainties have to be considered when converting the observed number $N_{2\nu \text{ECEC}}$ into a half-life (Extended Data Table 1). The 124Xe isotopic abundance in XENON1T was measured underground with a residual gas analyser with a systematic uncertainty of 1.5%. The resulting molar isotopic abundance of ¹²⁴Xe is $\eta = (9.94 \pm 0.14_{\text{stat}} + 0.15_{\text{sys}}) \times 10^{-4}$, which is 4% larger than the natural abundance³¹ of $\eta = (9.52 \pm 0.03) \times 10^{-4}$. The acceptance of the data selection criteria between 55 keV and 75 keV is constant within the uncertainties at $\epsilon = 0.967 \pm 0.007_{\text{stat}} \pm 0.033_{\text{sys}}$. The additional systematic uncertainty accounts for the fact that for a few data selection criteria only a lower limit on the acceptance was measurable. The finite resolution of the position reconstruction in XENON1T leads to an uncertainty on the fiducial mass. This was quantified by contrasting the mass fraction, derived from the fiducial volume geometry and LXe density³² of 2.862 g cm⁻³ at -96.1 °C, with the fraction of ^{ś3m}Kr events in the fiducial volume. With this, the fiducial mass is $m = (1,502 \pm 9_{\rm sys})$ kg. The half-life is then calculated as

$$T_{1/2}^{2\nu\text{ECEC}} = \ln 2 \frac{\epsilon \eta N_{\text{A}} mt}{M_{\text{Xe}} N_{2\nu\text{ECEC}}}$$

where $M_{\rm Xe}$ is the mean molar mass of xenon, $N_{\rm A}$ is Avogadro's constant and t is the live time of the measurement. The resulting half-life for the K-shell double electron capture of $^{124}{\rm Xe}$ is $T_{1/2}^{2\nu \rm ECEC} = (1.8 \pm 0.5_{\rm stat} \pm 0.1_{\rm sys}) \times 10^{22}$ yr. This is the longest half-life ever measured directly. Indications of a similarly long half-life for $2\nu \rm ECEC$ decay have been reported³ for $^{78}{\rm Kr}$. Within the uncertainties these half-lives are equally long, but the uncertainty of our result for $^{124}{\rm Xe}$ is about two times smaller. Furthermore, our result is compatible

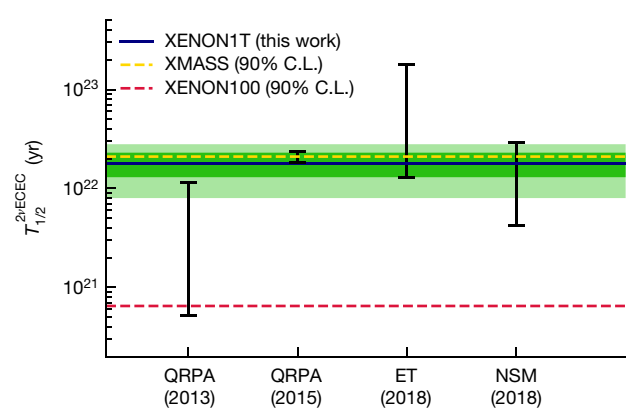


Fig. 4 | Observed 2νΕCEC half-life compared with theoretical predictions and other experiments. The measured half-life (solid blue) with the 1σ (2σ) statistical uncertainty band indicated in green (light green) is compared to the experimental 90% confidence level (C.L.) upper limits from XMASS⁷ (dashed yellow line) and XENON 100^{25} (dashed red line). Recent results from nuclear structure calculations^{8,13,14} for the 2ν ECEC show good agreement with the half-life measured in this work. The theoretical half-lives from the quasiparticle random-phase approximation (QRPA(2013)⁸ and QRPA(2015)¹³) were calculated for the double K-shell-electron (KK) capture (observed) as well as for electron captures from higher shells (not observed), so they have been scaled up by the KK fraction²¹ $f_{2\nu$ KK</sub> = 0.767 of the decay. The effective theory (ET¹⁴) and nuclear shell model (NSM¹⁴) half-lives for the double K-shell-electron capture are also shown.

with the lower limit from XMASS⁷ within the uncertainties (Fig. 4). With regard to nuclear theory, this measurement provides the first benchmark for nuclear structure models from the proton-rich side of the mass parabola. Predicted half-lives from recent nuclear calculations^{8,13,14}, which can now be refined further, are in the same window as the one observed (Fig. 4).

This first direct observation of $2\nu ECEC$ in ^{124}Xe also illustrates how xenon-based dark-matter search experiments, with their ever-growing target masses and simultaneously decreasing background levels, are becoming relevant for other rare event searches and neutrino physics. It sets the stage for $0\nu ECEC$ searches that can complement double- β -decay experiments in the hunt for the Majorana neutrino. Related processes involving the emission of one or two positrons $(2\nu EC\beta^+, 2\nu\beta^+\beta^+, 0\nu EC\beta^+, 0\nu\beta^+\beta^+)$ in ^{124}Xe might also exhibit interesting experimental signatures. The next-generation detectors XENONnT 18 , LZ^{19} and PandaX- $^{4}T^{33}$ are already under construction and will be able to probe these as-yet-unobserved decays with unprecedented sensitivity.

Online content

Any methods, additional references, Nature Research reporting summaries, source data, statements of data availability and associated accession codes are available at https://doi.org/10.1038/s41586-019-1124-4.

Received: 20 December 2018; Accepted: 6 March 2019; Published online 24 April 2019.

- Winter, R. G. Double K capture and single K capture with positron emission. Phys. Rev. 100, 142–144 (1955).
- 2. Gavrilyuk, Y. M. et al. Indications of $2\nu 2$ K capture in ⁷⁸Kr. *Phys. Rev. C* **87**, 035501 (2013).
- Ratkevich, S. S. et al. Comparative study of the double-K-shell-vacancy production in single- and double-electron-capture decay. *Phys. Rev. C* 96, 065502 (2017).
- Meshik, A. P., Hóhenberg, C. M., Pravdivtseva, O. V. & Kapusta, Y. S. Weak decay of ¹³⁰Ba and ¹³²Ba: geochemical measurements. *Phys. Rev. C* 64, 035205 (2001).
- Pujol, M., Marty, B., Burnard, P. & Philippot, P. Xenon in archean barite: weak decay of ¹³⁰Ba, mass-dependent isotopic fractionation and implication for barite formation. *Geochim. Cosmochim. Acta* 73, 6834–6846 (2009).
- Gavriljuk, Y. M. et al. 2K-capture in ¹²⁴Xe: results of data processing for an exposure of 37.7 kg day. *Phys. Part. Nucl.* 49, 563–568 (2018).



- Abe, K. et al. Improved search for two-neutrino double electron capture on $^{124}\rm{Xe}$ and $^{126}\rm{Xe}$ using particle identification in XMASS-I. Progr. Theor. Exp. Phys. **2018**, 053D03 (2018).
- Suhonen, J. Double beta decays of ¹²⁴Xe investigated in the QRPA framework. 8. J. Phys. G Nucl. Phys. 40, 075102 (2013).
- Aunola, M. & Suhonen, J. Systematic study of beta and double beta decay to
- excited final states. *Nucl. Phys. A* **602**, 133–166 (1996).

 10. Singh, S., Chandra, R., Rath, P. K., Raina, P. K. & Hirsch, J. G. Nuclear deformation and the two neutrino double-β-decay in ^{124,126}Xe, ^{128,130}Te, ^{130,132}Ba and ¹⁵⁰Nd isotopes. *Eur. Phys. J. A* **33**, 375–388 (2007).
- Hirsch, M., Muto, K., Oda, T. & Klapdor-Kleingrothaus, H. V. Nuclear structure calculation of $\beta^+\beta^+$, β^+ /EC and EC/EC decay matrix elements. Z. Phys. A **347**, 151-160 (1994).
- 12. Rumyantsev, O. A. & Urin, M. H. The strength of the analog and Gamow-Teller giant resonances and hindrance of the $2\nu\beta\beta$ -decay rate. Phys. Lett. B 443, 51–57 (1998).
- Pirinen, P. & Suhonen, J. Systematic approach to β and $2\nu\beta\beta$ decays of mass A = 100-136 nuclei. Phys. Rev. C 91, 054309 (2015).
- 14. Coello Pérez, E. A., Menéndez, J. & Schwenk, A. Two-neutrino double electron capture on 124Xe based on an effective theory and the nuclear shell model. Preprint at https://arxiv.org/abs/1809.04443 (2018).
- Majorana, E. Theory of the symmetry of electrons and positrons. *Nuovo Cimento* **14**, 171–184 (1937).
- Bernabeu, J., De Rujula, A. & Jarlskog, C. Neutrinoless double electron capture as a tool to measure the ν_e mass. *Nucl. Phys. B* **223**, 15–28 (1983). Sujkowski, Z. & Wycech, S. Neutrinoless double electron capture: a tool to
- search for Majorana neutrinos. Phys. Rev. C 70, 052501 (2004).
- Aprile, E. et al. Physics reach of the XENON1T dark matter experiment. J. Cosmol. Astropart. Phys. **1604**, 027 (2016).
- Mount, B. J. et al. LUX-ZEPLIN (LZ). Report No. LBNL-1007256 (Lawrence Berkeley National Laboratory, 2017).
- Aalbers, J. et al. DARWIN: towards the ultimate dark matter detector. J. Cosmol. Astropart. Phys. 1611, 017 (2016).
- Doi, M. & Kotani, T. Neutrinoless modes of double beta decay. Prog. Theor. Phys. 89, 139-159 (1993)
- Cullen, D. Program RELAX: A Code Designed to Calculate Atomic Relaxation Spectra of X-Rays and Electrons. Report No. UCRL-ID–110438 (Lawrence Livermore National Laboratory, 1992).
- Buchmüller, W., Peccei, R. & Yanagida, T. Leptogenesis as the origin of matter. Annu. Rev. Nucl. Part. Sci. 55, 311-355 (2005).
- Nesterenko, D. A. et al. Double-beta transformations in isobaric triplets with mass numbers A = 124, 130, and 136. Phys. Rev. C **86**, 044313
- Aprile, E. et al. Search for two-neutrino double electron capture of ¹²⁴Xe with XENON100. Phys. Rev. C 95, 024605 (2017).
- Aprile, E. et al. The XENON1T dark matter experiment. Eur. Phys. J. C 77, 881 (2017)
- Aprile, E. et al. Dark matter search results from a one tonne x year exposure of XENON1T. Phys. Rev. Lett. 121, 111302 (2018).
- 28. Aprile, E. et al. Conceptual design and simulation of a water Cherenkov muon veto for the XENON1T experiment. J. Instrum. 9, P11006 (2014)
- Aprile, E. et al. Material radioassay and selection for the XENON1T dark matter experiment. Eur. Phys. J. C 77, 890 (2017).
- Aprile, E. et al. Removing krypton from xenon by cryogenic distillation to the ppq level. Eur. Phys. J. C 77, 275 (2017).
- de Laeter, J. et al. Atomic weights of the elements. Review 2000 (IUPAC technical report). Pure Appl. Chem. 75, 683-800 (2003).
- Linstrom, P. & Mallard, W. G. E. NIST Chemistry WebBook, NIST Standard Reference Database Number 69 https://doi.org/10.18434/T4D303 (2018)
- Zhang, H. et al. Dark matter direct search sensitivity of the PandaX-4T experiment. Sci. China Phys. Mech. Astron. 62, 31011 (2019).

Acknowledgements We thank J. Menéndez for sharing his expertise in the theory of double $\boldsymbol{\beta}$ decay. We gratefully acknowledge support from the National Science Foundation, Swiss National Science Foundation, German Ministry for Education and Research, Max Planck Gesellschaft, Deutsche Forschungsgemeinschaft, Netherlands Organisation for Scientific Research (NWO), NLeSC, Weizmann Institute of Science, I-CORE, Pazy-Vatat, Initial Training Network Invisibles (Marie Curie Actions, PITNGA-2011-289442) Fundação para a Ciencia e a Tecnologia, Region des Pays de la Loire, Knut and Alice Wallenberg Foundation, Kavli Foundation, Abeloe Graduate Fellowship, and Istituto Nazionale di Fisica Nucleare. Data processing was performed using infrastructures of the Open Science Grid and European Grid Initiative. We are grateful to Laboratori Nazionali del Gran Sasso for hosting and supporting the XENON project. B.K. was also at Albert Einstein Center for Fundamental Physics, University of Bern, Bern, Switzerland. S.K. is also at Kobayashi-Maskawa Institute, Nagoya University, Nagoya, Japan. J.A.M.L. is also at Coimbra Polytechnic - ISEC, Coimbra, Portugal.

Reviewer information Nature thanks Jouni Suhonen and the other anonymous reviewer(s) for their contribution to the peer review of this work.

Author contributions The XENON1T detector was designed and constructed by the XENON Collaboration. Operation, data processing, calibration, Monte Carlo simulations of the detector and of theoretical models, and data analyses were performed by a large number of XENON Collaboration members, who also discussed and approved the scientific results. The paper was written by A.F. and C. Wittweg. It was reviewed and edited by the collaboration and all authors approved the final version of the manuscript.

Competing interests The authors declare no competing interests.

Additional information

Extended data is available for this paper at https://doi.org/10.1038/s41586-019-1124-4

Reprints and permissions information is available at http://www.nature.com/ reprints.

Publisher's note: Springer Nature remains neutral with regard to jurisdictional claims in published maps and institutional affiliations.

© The Author(s), under exclusive licence to Springer Nature Limited 2019

XENON Collaboration*

E. Aprile¹, J. Aalbers^{2,3}, F. Agostini⁴, M. Alfonsi⁵, L. Althueser⁶, F. D. Amaro⁷, M. Anthony¹, V. C. Antochi², F. Arneodo⁸, L. Baudis⁹, B. Bauermeister², M. L. Benabderrahmane⁸, T. Berger¹⁰, P. A. Breur³, A. Brown⁹, A. Brown³, E. Brown¹⁰, S. Bruenner¹¹, G. Bruno⁸, R. Budnik¹², C. Capelli⁹, J. M. R. Cardoso⁷, D. Cichon¹¹, D. Coderre¹³, A. P. Colijn³, J. Conrad², J. P. Cussonneau¹⁴, M. P. Decowski³, P. de Perio¹, P. Di Gangi⁴, A. Di Giovanni⁸, S. Diglio¹⁴, A. Elykov¹³, G. Eurin¹¹, J. Fei¹⁵, A. D. Ferella², A. Fieguth^{6*}, W. Fulgione^{16,17}, A. Gallo Rosso¹⁶, M. Galloway⁹, F. Gao¹, M. Garbini⁴, L. Grandi¹⁸, Z. Greene¹, C. Hasterok¹¹, E. Hogenbirk³, J. Howlett¹, M. lacovacci¹⁹, R. Itay¹², F. Joerg¹¹, B. Kaminsky¹³, S. Kazama⁹, A. Kish⁹, G. Koltman¹², A. Kopec²⁰, H. Landsman¹², R. F. Lang²⁰, L. Levinson¹², Q. Lin¹, S. Lindemann¹³, M. Lindner¹¹, F. Lombardi¹⁵, J. A. M. Lopes⁷, E. López Fune²¹, C. Macolino²², J. Mahlstedt², A. Manfredini^{9,12}, F. Marignetti¹⁹, T. Marrodán Undagoitia¹¹, J. Masbou¹⁴, D. Masson²⁰, S. Mastroianni¹⁹, M. Messina⁸, K. Micheneau¹⁴, K. Miller¹⁸, A. Molinari¹⁶, K. Morå², M. Murra⁶, J. Naganoma^{16,23}, K. Ni¹⁵, U. Oberlack⁵, K. Odgers¹⁰, B. Pelssers², R. Peres^{7,9}, F. Piastra⁹, J. Pienaar¹⁸, V. Pizzella¹¹, G. Plante¹, R. Podviianiuk¹6, N. Priel¹², H. Qiu¹², D. Ramírez García¹³, S. Reichard³, B. Riedel¹8, A. Rizzo¹, A. Rocchetti¹³, N. Rupp¹¹, J. M. F. dos Santos³, G. Sartorelli⁴, N. Šarčeviċ¹³, M. Scheibelhut⁵, S. Schindler⁵, J. Schreiner¹¹, D. Schulte⁶, M. Schumann¹³, L. Scotto Lavina²¹, M. Selvi⁴, P. Shagin²³, E. Shockley¹⁸, M. Silva⁷, H. Simgen¹¹, C. Therreau¹⁴, D. Thers¹⁴, F. Toschi¹³, G. Trinchero¹⁷, C. Tunnell^{18,23}, N. Upole¹⁸, M. Vargas⁶, O. Wack¹¹, H. Wang²⁴, Z. Wang¹⁶, Y. Wei¹⁵, C. Weinheimer⁶, D. Wenz⁵, C. Wittweg^{6*}, J. Wulf⁹, J. Ye¹⁵, Y. Zhang¹, T. Zhu¹ & J. P. Zopounidis²¹

¹Physics Department, Columbia University, New York, NY, USA. ²Oskar Klein Centre, Department of Physics, Stockholm University, AlbaNova, Stockholm, Sweden. 3Nikhef and the University of Amsterdam, Science Park, Amsterdam, The Netherlands. ⁴Department of Physics and Astronomy, University of Bologna and INFN-Bologna, Bologna, Italy. ⁵Institut für Physik & Exzellenzcluster PRISMA, Johannes Gutenberg-Universität Mainz, Mainz, Germany. ⁶Institut für Kernphysik, Westfälische Wilhelms-Universität Münster, Münster, Germany, ⁷LIBPhys, Department of Physics, University of Coimbra, Coimbra, Portugal. ⁸New York University Abu Dhabi, Abu Dhabi, United Arab Emirates. 9Physik-Institut, University of Zurich, Zurich, Switzerland. 10 Department of Physics, Applied Physics and Astronomy, Rensselaer Polytechnic Institute, Troy, NY, USA. ¹¹Max-Planck-Institut für Kernphysik, Heidelberg, Germany. ¹²Department of Particle Physics and Astrophysics, Weizmann Institute of Science, Rehovot, Israel. ¹³Physikalisches Institut, Universität Freiburg, Freiburg, Germany. ¹⁴SUBATECH, IMT Atlantique, CNRS/IN2P3, Université de Nantes, Nantes, France. ¹⁵Department of Physics, University of California, San Diego, CA, USA. ¹⁶INFN-Laboratori Nazionali del Gran Sasso and Gran Sasso Science Institute, L'Aquila, Italy. ¹⁷INFN-Torino and Osservatorio Astrofisico di Torino, Torino, Italy. 18 Department of Physics & Kavli Institute for Cosmological Physics, University of Chicago, Chicago, IL, USA. ¹⁹Department of Physics 'Ettore Pancini', University of Napoli and INFN-Napoli, Naples, Italy. ²⁰Department of Physics and Astronomy, Purdue University, West Lafayette, IN, USA. ²¹LPNHE, Sorbonne Université, Université Paris Diderot, CNRS/IN2P3, Paris, France. ²²LAL, Université Paris-Sud, CNRS/IN2P3, Université Paris-Saclay, Orsay, France. ²³Department of Physics and Astronomy, Rice University, Houston, TX, USA. ²⁴Physics and Astronomy Department, University of California, Los Angeles, CA, USA. *e-mail: xenon@lngs.infn.it; a.fieguth@uni-muenster.de; c.wittweg@uni-muenster.de

METHODS

Selection of the fiducial mass. Because the 2ν ECEC signal is proportional to the number of 124 Xe nuclei, it grows linearly with the xenon mass of the volume selected for the analysis, $m_{\rm volume}$. The ability to distinguish signal events from background depends on the background uncertainty $\Delta N_{\rm background}$. For a counting experiment, the uncertainty on the number of background events $N_{\rm background}$ is of Poissonian nature, so $\Delta N_{\rm background} = \sqrt{N_{\rm background}}$. The discovery sensitivity in a detector volume $S_{\rm vol}$ is then proportional to the xenon mass in the selected volume divided by the background uncertainty:

$$S_{\rm vol} \propto \frac{m_{\rm volume}}{\sqrt{N_{\rm background}}}$$
 (1)

The S_{vol} parameter was optimized using an automated algorithm that tests both cylindrical and superellipsoidal volumes. A 1,502-kg-mass superellipsoid was found to give the optimal sensitivity. Because the signal region was blinded, the optimization was carried out in an energy sideband from 80 keV to 140 keV. For the fit of Monte Carlo simulations to the measured energy spectrum and consistency checks, the volume was segmented into an inner and outer volume (as indicated in Extended Data Fig. 1). Intrinsic background sources mixed with the xenon, solar neutrinos and the 2ν ECEC signal are expected to show the same activity in both volumes. However, the contribution from detector material backgrounds is strongest near the outer surfaces of these volumes. Fitting both volumes simultaneously gives a more robust fit and higher sensitivity than fitting a single monolithic volume. **Energy calibration and resolution.** Monoenergetic lines from the γ decays of four different isotopes were used for the energy calibration of the XENON1T detector. ^{83m}Kr is a gaseous calibration source that is homogeneously distributed inside the detector³⁴. The isomer undergoes a multi-step decay that is highly converted and deposits 41.5 keV inside the detector. This represents the lowest monoenergetic calibration point. The metastable isotopes ^{131m}Xe (163.9 keV) and ^{129m}Xe (236.2 keV) were neutron-activated during the calibration campaigns and decay with half-lives of 11.86 d and 8.88 d, respectively. The 1,173.2-keV and 1,332.5-keV transitions of ⁶⁰Co, which is present in the stainless steel detector components, such as the cryostat, are the highest energy calibration lines. Only energy depositions where the total energy of the γ transition is deposited in a single resolvable interaction within the detector that is, the full absorption peak—were taken into account. The S1 and S2 signals from these interactions were then used to determine the yields of light and charge per unit energy for each source. These two quantities are anti-correlated 35,36, resulting in:

$$E = W \times \left[\frac{cS1}{g_1} + \frac{cS2_b}{g_2} \right] \tag{2}$$

at a given energy E. Here, $W=(13.7\pm0.2)~{\rm eV}$ is the average energy 37 needed to generate measurable quanta in LXe (S1 photons or S2 electrons), and cS1 and $cS2_{\rm b}$ are the measured S1 and S2 signals corrected for detector effects. S1 is corrected for the spatially dependent S1 light collection efficiency, whereas S2 is corrected for the spatial dependencies of both the charge amplification and the S2 light collection efficiency. The subscript on $cS2_{\rm b}$ identifies the S2 signal seen by the bottom PMT array, which was used for energy reconstruction to minimize the impact of signal saturation and non-uniformity due to single inactive PMTs in the top array. A fit to the measured data points gives the detector-specific calibration parameters g_1 and g_2 . The calibration procedure was carried out in ten slices along the central axis of the cylindrical detector to account for the depth dependence of $g_1(z)$ and $g_2(z)$ for the energy reconstruction.

The energy resolution was determined from the reconstructed spectrum by fitting Gaussian functions with the mean energy $\mu_{\rm E}$ and standard deviation $\sigma_{\rm E}$ to monoenergetic peaks of the calibration sources (^{83m}Kr, ^{131m}Xe, ^{129m}Xe) and radioactive isotopes in the TPC materials (²¹⁴Pb, ²⁰⁸Tl) up to 510.8 keV. The relative resolution is then given by $\sigma_{\rm E}/\mu_{\rm E}$ for each peak. Finally, the data points are fitted with a phenomenological function:

$$\frac{\sigma_{\rm E}}{\mu_{\rm E}} = \frac{a}{\sqrt{E}} + b \tag{3}$$

which gives an energy resolution of 4.1% at the 2ν ECEC energy (Extended Data Fig. 2).

Iodine removal. Thermal neutrons can be captured by ¹²⁴Xe, producing ¹²⁵Xe:

$$^{124}Xe + n \rightarrow ^{125}Xe + \gamma \tag{4}$$

¹²⁵Xe decays to ¹²⁵I via electron capture with a half-life of 16.9 h:

$$\stackrel{125}{\text{Xe}} \xrightarrow{16.9\text{h}} \stackrel{125}{\longrightarrow} I^* + \nu_{\text{e}}$$

$$\stackrel{125}{I^*} \xrightarrow{\leq 1 \text{ns}} \stackrel{125}{\longrightarrow} I + \gamma + X$$
(5)

where X denotes the X-rays and Auger electrons emitted from the atomic relaxation after the electron capture. Iodine also undergoes electron capture to 125 Te with a 59.4-d half-life:

Both decays populate short-lived excited nuclear states of ^{125}I and ^{125}Te , and the signals from the γ transitions are merged with the atomic relaxation signals following the electron capture. The Te K-shell X-ray, which has a branching ratio of 87.5%, is merged with a 35.5-keV nuclear transition. This is problematic because it creates a Gaussian line centred around 67.3 keV, which is about 1σ away from the 64.3 keV expected for $2\nu\text{ECEC}$.

Two main mechanisms leading to the presence of ¹²⁵I in the detector have been identified: (1) artificial activation during calibration campaigns using neutrons from the deuterium–deuterium–fusion neutron generator or the ²⁴¹AmBe source and (2) activation outside the water shield by environmental thermal neutrons. As the decay rate of ¹²⁵Xe can be monitored during and after calibration, one can predict the decay rate of its iodine daughter. For environmental neutrons, flux measurements at Laboratori Nazionali del Gran Sasso were used to estimate the activation. These estimates were cross-checked with the ¹²⁵Xe decay peaks in the data. In the analysis of both the AmBe and the neutron generator data, fewer iodine decays than expected from the decay of the mother isotope ¹²⁵Xe were found. This is attributed to the removal of ¹²⁵I during the continuous purification of the detector's xenon inventory by circulation over hot zirconium getters. Owing to the blinding of the signal region containing the ¹²⁵I peak, the long-term behaviour of this removal could only be assessed after unblinding.

Because every ^{125}Xe decay in the detector leads to the presence of an ^{125}I nucleus, a model was constructed for the expected iodine decay rate from artificial activation by integrating the background-subtracted ^{125}Xe rate over time in one-day steps. The data were then convolved with the effective decay constant τ and fitted with a free amplitude and a linear background to the measured ^{125}I rate evolution in a 2σ interval around the peak (61.7–72.9 keV). An effective ^{125}I decay constant of $\tau=(9.1\pm2.6)$ d was found, which is in agreement with the expected decay constant from completely efficient getter removal.

Because the model was constructed directly from data, the uncertainties from the $^{125}\mathrm{Xe}$ rates were propagated by introducing artificial Poisson fluctuations to the data points. An $^{125}\mathrm{I}$ model was made for each variation of the $^{125}\mathrm{Xe}$ data and fitted to the $^{125}\mathrm{I}$ rate evolution. The best fit to the $^{125}\mathrm{I}$ rate over time in 10-d bins and the uncertainty band derived from an ensemble of 1,000 fits are shown in Extended Data Fig. 3. Different binnings of 1–14 d were tested for consistency with χ^2 and log-likelihood fits.

Integration of each model over the actual data-taking periods yielded an expected number of $^{125}\mathrm{I}$ decays $N_{125_{\mathrm{I},\mathrm{art}}}$. The ensemble distribution of $N_{125_{\mathrm{I},\mathrm{art}}}$ allowed us to extract both a central value and uncertainties. Only datasets with decay rates at the non-activated background level were selected for the $2\nu ECEC$ search. The final data selection is shown in Extended Data Fig. 3. For the spectral fit of the remaining live time of 177.7 d we constrained the number of expected iodine events from artificial activation $N_{125_{\mathrm{I},\mathrm{rad}}}$ using the model. We also constrained the radiogenic component $N_{125_{\mathrm{I},\mathrm{rad}}}$ by taking into account the effective decay constant τ .

Fitting method and result. The data were fitted with all known background sources, either simulated or modelled as Gaussian peaks, and the 2ν ECEC peak. The scaling parameters of the simulated Monte Carlo spectra and the properties of the Gaussian peaks are the fit parameters in the χ^2 minimization:

$$\chi_{\text{combined}}^{2}(\boldsymbol{p}) = \sum_{i} \frac{[R_{i} - f(E_{i}, \boldsymbol{p})]^{2}}{(\Delta R_{i})^{2}}$$
 (7)

where R_i is the measured event rate in the energy bin E_i and $f(E_b, p)$ is the background fit function. At energies below 100 keV, the low statistics of the simulated backgrounds from the detector construction materials require an interpolation of the simulated spectra in order to avoid over-fitting. Because the main background contribution from materials in this energy region is from single Compton scatters from γ -rays in the sensitive volume, a featureless spectrum is expected. Therefore, the sum of material contributions was linearly interpolated up to 100 keV. This gives:

$$f(E_{i}, \mathbf{p}) = \left[\sum_{k}^{\text{materials}} p_{k} R_{k}(E_{i})\right]_{\text{interpolated} < 100 \text{ keV}} + \sum_{l}^{\text{intrinsic}} p_{l} R_{l}(E_{i}) + \sum_{m}^{\text{Gaussians}} Gaussian_{m}(\mathbf{p}_{m}, E_{i})$$
(8)



where the sums correspond to the interpolated material component, the intrinsic sources plus solar neutrinos and the Gaussian peaks, with fit parameters $p_{k,l,m} \in p$. Knowledge from external measurements, such as material screening²⁹, ⁸⁵Kr concentration measurements²⁷ and elemental abundances, were incorporated into the fit function and constrained using terms of the form:

$$constraint_{j} = \frac{(parameter_{j} - expectation_{j})^{2}}{uncertainty_{j}^{2}}$$
(9)

A deviation of the fit parameter from the expectation by $n \times \sigma$ will thus increase the value of the χ^2 function by n^2 . The Gaussian signal peak was constrained in the fit as well given the prior information on the expected position and width. Moreover, systematic uncertainties from the cut acceptance and fiducial mass were addressed by including these as constrained fit parameters in the fit function. As the fit was carried out in an inner (1.0 t; fit range 10–300 keV) and outer (0.5 t; fit range 10–200 keV) detector volume, each of the two volumes has its own χ^2 function with distinct parameters for the respective fiducial masses V and cut acceptances κ . The energy reconstruction was found to agree within the uncertainties. The full χ^2 function can then be written as:

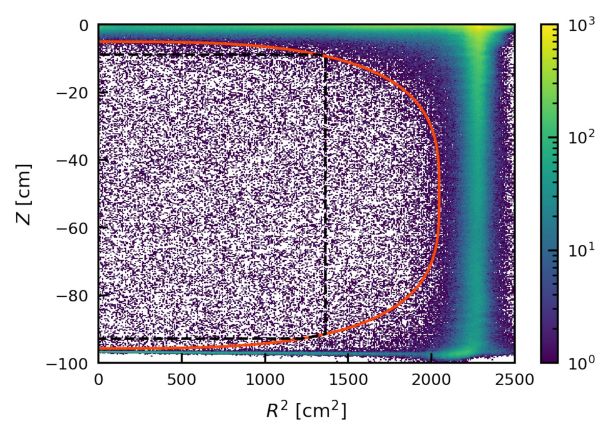
$$\chi^{2}_{\text{combined}}(\boldsymbol{p}, \boldsymbol{V}, \boldsymbol{\kappa}) = \chi^{2}_{\text{inner}}(\boldsymbol{p}, V_{\text{inner}}, \kappa_{\text{inner}}) + \chi^{2}_{\text{outer}}(\boldsymbol{p}, V_{\text{outer}}, \kappa_{\text{outer}}) + \text{constraint}_{\boldsymbol{p}} + \text{constraint}_{\boldsymbol{V}} + \text{constraint}_{\kappa}$$
(10)

More details of the background modelling will be provided in a future publication. The χ^2 curve for the number of observed 2ν ECEC events is shown in Extended Data Fig. 4. The 4.4σ significance is derived from the difference in $\Delta\chi^2$ between the best fit and a null result along the curve.

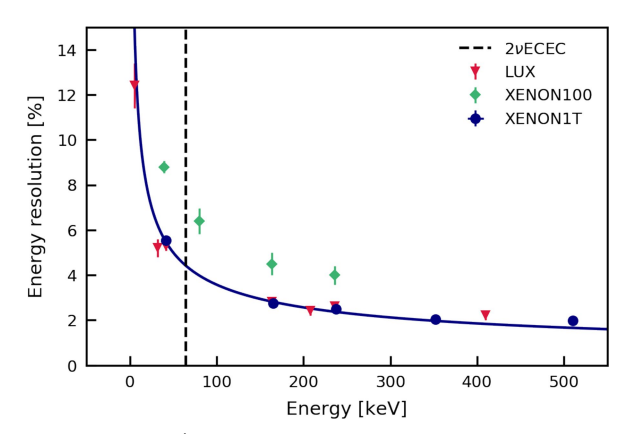
Data availability

The data that support the findings of this study are available from the corresponding authors upon reasonable request.

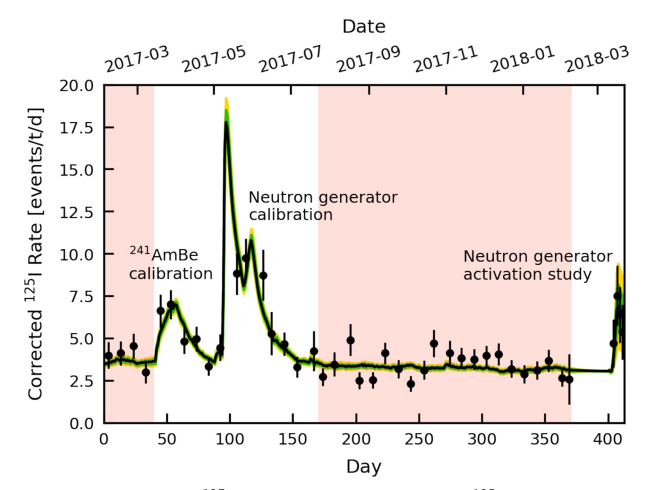
- Manalaysay, A. et al. Spatially uniform calibration of a liquid xenon detector at low energies using ^{83m}Kr. Rev. Sci. Instrum. 81, 073303 (2010).
- 35. Conti, É. et al. Correlated fluctuations between luminescence and ionization in liquid xenon. *Phys. Rev. B* **68**, 054201 (2003).
- Aprile, E., Giboni, K. L., Majewski, P., Ni, K. & Yamashita, M. Observation of anti-correlation between scintillation and ionization for MeV gamma-rays in liquid xenon. *Phys. Rev. B* 76, 014115 (2007).
- Szydagis, M. et al. NEST: a comprehensive model for scintillation yield in liquid xenon. J. Instrum. 6, P10002 (2011).
- Akerib, D. S. et al. Signal yields, energy resolution, and recombination fluctuations in liquid xenon. *Phys. Rev. D* 95, 012008 (2017).
- Aprile, E. et al. The XENON100 dark matter experiment. Astropart. Phys. 35, 573–590 (2012).



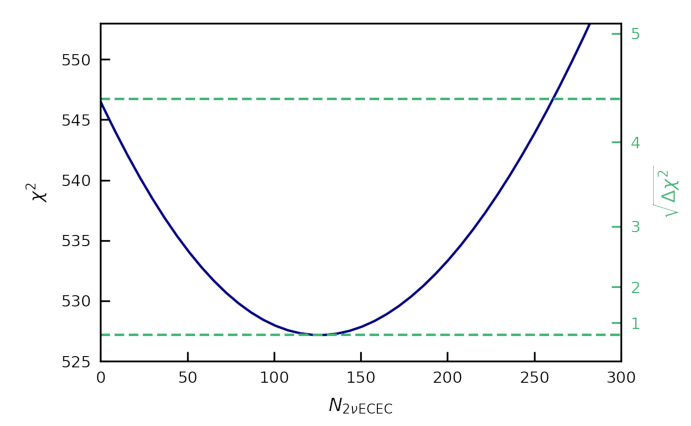
Extended Data Fig. 1 | Spatial distribution of events. Interaction depth Z versus squared radius R^2 for events with energies 80–140 keV. High-density areas correspond to the edges of the TPC, where most of external β and γ radiation is absorbed. The 1,502-kg fiducial volume is indicated by the solid red line. Further segmentation into an inner (1.0 t) and an outer (0.5 t) volume is marked by the black dashed line.



Extended Data Fig. 2 | **Energy resolution.** Ratio of the mean peak energy ($\mu_{\rm E}$) to the peak width ($\sigma_{\rm E}$) for low-energy monoenergetic lines in selected LXe dark-matter experiments (LUX³⁸ and XENON100³⁹) and in the 1.5-t fiducial mass of the XENON1T detector. The relative resolution is defined as the $\sigma_{\rm E}/\mu_{\rm E}$ ratio of the Gaussian lines and is fitted using a phenomenological function (solid blue line). For XENON1T the data points are ^{83m}Kr (41.5 keV), ^{131m}Xe (163.9 keV), ^{129m}Xe (236.2 keV), ²¹⁴Pb (351.9 keV) and ²⁰⁸Tl (510.8 keV). Only statistical uncertainties are shown for XENON1T (smaller than the markers). The energy of the 2ν ECEC peak is indicated by the black dashed line.



Extended Data Fig. 3 | ¹²⁵**I time evolution.** Fit of the ¹²⁵**I** model to data in a 2σ energy interval around the mean energy of the ¹²⁵**I** peak in 10-d bins with Poisson uncertainties. Periods with an increased ¹²⁵**I** decay rate are attributed to artificial activations from neutron calibrations, equipment tests and a dedicated activation study. The decrease of the rate to the background level corresponds to an effective iodine decay constant of $\tau=9.1$ d. The best fit is shown as a solid black line. The green (yellow) bands mark the 1σ (2σ) model uncertainties resulting from the Poisson uncertainties of the ¹²⁵Xe data underlying the model. The pink bands indicate the data selection for the 2ν ECEC search, where the decay rate has returned to the background level.



Extended Data Fig. 4 | χ^2 curve for the number of measured 2ν ECEC events. By comparing the best-fit value of $N_{2\nu$ ECEC} = 126 events to a null result one obtains $\sqrt{\Delta\chi^2} = 4.4$.



Extended Data Table 1 | Systematic uncertainties

a) Variable in $T_{1/2}^{\sf ECEC}$ calculation	Uncertainty [%]	
Fiducial mass m	0.6	
ROI cut acceptance ϵ	3.4	
$^{124}\mathrm{Xe}$ abundance η	1.5	
b) Constrained fit parameter	Value \pm uncertainty	Parameter pull $[\sigma]$
v_{solar} multiplier	1.00 ± 0.20	0.3
$^{136}{ m Xe}~2 uetaeta$ multiplier	1.00 ± 0.05	-0.2
Volume _{inner,outer} multipliers	1.00 ± 0.01	$0.7_{\mathrm{inner}}, \ -0.7_{\mathrm{outer}}$
High energy acceptance inner, outer multipliers	0.67 ± 0.33	$0.1_{\rm inner},\ -1.0_{\rm outer}$
$^{85}{ m Kr}$ concentration	$(0.66 \pm 0.12)~\mathrm{ppt}~^{\mathrm{nat}}\mathrm{Kr/Xe}$	0.3
$N_{125}{}_{ m I}$	(10 ± 7) events	-0.2
$\mu_{125}{}_{ m I}$	$(67.3 \pm 0.5)~\text{keV}$	-0.1
$\sigma_{125}{}_{ m I}$	$(2.8\pm0.5)~\mathrm{keV}$	-0.1
$\mu_{2 uECEC}$	$(64.3 \pm 0.6)~\text{keV}$	-0.3
$\sigma_{2 u}$ ecec	$(2.6\pm0.3)~\mathrm{keV}$	-0.2
$\mu_{83m_{\mathrm{Kr},1}}$	$(32.2\pm0.6)~\text{keV}$	0.7
$\mu_{83m_{\mathrm{Kr},2}}$	$(41.5\pm0.6)~\mathrm{keV}$	-0.1
$\mu_{131m_{\mathrm{Xe}}}$	$(163.9 \pm 0.6)~\text{keV}$	2.4
$\mu_{129m_{\mathrm{Xe}}}$	$(236.2\pm0.6)~\text{keV}$	1.0

a, Uncertainties in the half-life calculation are given as percentages of the corresponding variable values. b, Systematic uncertainties incorporated as fit constraints are given in the unit used in the fit. All parameters are shared between the χ^2 functions for both volumes, with the exception of the volume and high-energy acceptance multipliers. The volume multipliers are chosen such that the fitted high-energy acceptance ranges between the lower limit derived from the data and unity. The parameter pulls of the fit are given in units of the uncertainty σ . ROI, region of interest; ppt, parts per trillion; T_1^{ECEC} , $2\nu\text{ECEC}$ half-life.